

**LOW TEMPERATURE HEAT-TREATMENT CYCLE ON AlSi10Mg_200C ALLOY
FABRICATED BY DIRECT LASER METAL SINTERING:
MICROSTRUCTURE EVOLUTION AND CORROSION RESISTIVITY**

*M. Rafieazad¹, P. Fathi¹, M. Mohammadi², and A.M. Nasiri¹

¹*Faculty of Engineering and Applied Science, Memorial University of Newfoundland, St. John's, NL,
Canada, A1B 3X5*

(*Corresponding author: mrafieazad@mun.ca)

²*Marine Additive Manufacturing Centre of Excellence (MAMCE), University of New Brunswick, 3 Bailey
Drive, P.O. Box 4400, Fredericton, NB, Canada, E3B 5A3*

ABSTRACT

This study examines the impact of low-temperature heat-treatment cycles on microstructure and corrosion performance of Direct Metal Laser Sintered (DMLS) AlSi10Mg_200C alloy. It is known that the morphology and the size of eutectic silicon are the two most critical factors affecting mechanical properties of the AlSi10Mg alloy. Although high-temperature heat-treatment cycles are common practice for the strengthening of the cast Al-Si-Mg alloys, in the case of DMLS fabricated AlSi10Mg alloy, high-temperature solutionizing and low temperature annealing cycles result in mechanical properties degradation primarily due to a dramatic decrease in the solubility of Si in the super-saturated α -Al matrix of the as-printed alloy. In this study, low-temperature heat-treatment cycles that only promote precipitation of Mg₂Si accompanied by the interruption of the silicon network were investigated. SEM and XRD analysis were utilized to observe the evolution of microstructure after different annealing heat-treatments at 200, 250, 300, and 350°C for 3 h. Increasing the heat-treatment temperature contributed to the Si networks interruption and an increased precipitation of Mg₂Si phase. Low-temperature annealing from 200 to 350°C was found to promote the homogeneity of the microstructure characterized by a uniform distribution of eutectic Si in α -Al matrix. Additionally, in order to investigate the impact of different heat-treatment cycles on corrosion resistivity of DMLS-AlSi10Mg_200C, the potentiodynamic polarization testing and electrochemical impedance spectroscopy were performed in a 3.5 wt.% NaCl solution. The results revealed more uniformly distributed pitting attack on the corroded surface by further increase in the annealing temperature, which was attributed to the uniformity of Si dispersion. In comparison, low temperature annealing at 200°C led to a penetrating selective corrosion attack along the melt pool boundaries, resulting in a higher corrosion rate associated with the lower absolute value of impedance of the protective passive film on the surface.

KEYWORDS

Direct metal laser sintering, Corrosion resistivity, AlSi10Mg, Heat-treatment, Microstructure

INTRODUCTION

The ever-present need for advanced engineering components with a complex design and exceptional mechanical performance requires the implementation of innovative manufacturing technologies. In this regard, additive manufacturing (AM) technology is gaining more attention thanks to its innovative freedom to design complicated and near-net shapes, mostly without any geometrical constraint, and saving material due to lack of scrap, and efficient products fabrication with lower costs within a few hours (Asgari, Baxter, Hosseinkhani, & Mohammadi, 2017).

Aluminum alloys containing Silicon and Magnesium as the primary alloying elements have conceived a lightweight alloy family owning proper mechanical properties as well as corrosion performance (Li, Wang, Jie, & Wei, 2011). Among a wide variety of alloys in this family, AlSi10Mg has been mostly adapted by the AM industry, and in particular through Direct Metal Laser Sintering (DMLS) process. AlSi10Mg as a hypo-eutectic alloy has multiplicity of applications in the aerospace and automotive industries due to its distinctive properties (Fulcher, Leigh, & Watt, 2014).

The unique process conditions during DMLS, such as rapid solidification resulted from extremely high cooling rates of small melt pools, produce a fine microstructure and a large amount of residual thermal stresses within the structure, which can create dimensional inaccuracy or distortion in the printed part. For this reason, annealing heat-treatment is commonly utilized to avoid part's distortion and release some of the residual stresses (Manfredi et al., 2013). However, previous studies show that high-temperature heat-treatment cycles promote modification in the microstructure of DMLS-AlSi10Mg alloy at the expense of losing mechanical properties (Aboulkhair, Tuck, Ashcroft, Maskery, & Everitt, 2015). In another study, it was reported that increasing annealing temperature for this alloy decreases the solubility of Si in Al matrix and contributes to the coalescence of Si particles, resulting in a decrease in hardness and tensile strength, whereas the elongation was found to increase significantly (Mertens, Dedry, Reuter, Rigo, & Lecomte-Beckers, 2015). From this perspective, heat-treatment can be applied to optimize and tune mechanical properties of the DMLS-AlSi10Mg alloy, through microstructural modifications (Ma et al., 2014).

High-temperature annealing at 823 K for four hours on DMLS-AlSi10Mg alloy was reported to form a uniform microstructure composed of coarse Si particles within the α -Al matrix (Cabrini et al., 2016). Consequently, an active behavior and a decreased corrosion resistivity of the alloy characterized by a severe localized corrosion in the Al matrix surrounded the coarse Si particles was reported after the heat-treatment (Cabrini et al., 2016). On the other hand, the un-treated DMLS-AlSi10Mg sample and the stress-relieved ones, due to the increased content of the Si and the breakage of its network along the heat affected zones, were reported to exhibit localized and selective attacks preferentially along the melting pools boundaries (Cabrini et al., 2016).

There are very limited information available in open literature on the post heat-treatment of DMLS-AlSi10Mg components, particularly on the effects of thermal treatments on electrochemical properties of the alloy. This paper is the first research article that investigates the impact of low-temperature heat-treatments on the corrosion performance of the DMLS-AlSi10Mg_200C alloy. It focuses on the microstructural evolution and the resulting corrosion properties of the alloy upon low temperature annealing at 200, 250, 300, and 350°C. This study is essential in designing low temperature-low cost thermal treatments specific to the DMLS produced components to obtain a balanced set of corrosion-mechanical properties.

EXPERIMENTAL PROCEDURE

Materials

In this study, AlSi10Mg_200C cubes with $10 \times 10 \times 10$ mm dimensions were employed. These cubes were produced using an EOS M290 metal 3D printer machine equipped with a 400 W Yb-fibre laser with 100 μ m spot size. The used gas atomized AlSi10Mg_200C powders in this study had an average particle size distribution of 8.8 ± 7 μ m with a chemical composition given in Table 1.

Table 1. Chemical compositions of AlSi10Mg_200C powder (wt. %)

Si	Mg	Fe	Mn	Ti	Zn	Cu	Al
9.00-11.00	0.20- 0.45	≤0.55	≤0.45	≤0.15	≤0.10	≤0.05	Bal.

Heat-Treatment of DMLS-AlSi10Mg_200C Specimens

After the fabrication process, samples were subjected to the low-temperature annealing for 3 h at four different temperatures, *i.e.*, 200, 250, 300, and 350°C, in an Argon atmosphere to minimize the oxidation during the heat-treatment. This was followed by water quenching of the heat-treated samples to the room temperature.

Microstructure Characterization

For microstructure characterization of the samples, all DMLS-samples were sectioned along both the building plane and the building direction, followed by standard grinding and polishing procedures utilizing a Tegramin-3 Struers auto-grinder/polisher. Then, Keller etchant (2.5 vol.% HNO₃, 1 vol.% HF, 1.5 vol.% HCl, and 95 vol.% H₂O) was used to reveal the microstructure. The microstructure of all samples was characterized using an optical microscope (Nikon Eclipse 50i) and a scanning electron microscope (SEM) (FEI MLA 650F). Phase characterization of the samples after each heat-treatment was determined using a Rigaku Ultimate IV X-ray diffraction (XRD) with Cu-K_α source at 40 kV and 44 mA at the diffraction angle range of 20–50° with a step size of 0.02°.

Potentiodynamic Polarization Test

Electrochemical measurements of all the polished DMLS-produced samples were conducted using an IVIUM CompactStat™ Potentiostat with a three-electrode cell setup based on the ASTM G5 standard for potentiodynamic polarization measurements (ASTM-G5-82, 1982). The samples were immersed in a 3.5 wt.% NaCl solution to simulate seawater corrosion conditions at 25°C. The potential range for the Tafel curve measurements was applied from -0.3 V to +0.3 V employing scanning rate of 0.125 mV/s. After corrosion product removal using concentrated HNO₃ solution (15.8 N) in an ultrasonic bath for 20 min, the corrosion morphology was investigated using the SEM.

Electrochemical Impedance Spectroscopy (EIS) Test

EIS test was also carried out on polished samples every 24 h of immersion time in 3.5 wt.% NaCl solution for five consecutive days. Signals with 0.01 V amplitude over the open circuit potential with a frequency range between 10000 Hz and 10⁻² Hz were applied. All corrosion tests were carried out on the polished surfaces to only evaluate the effect of microstructure and heat-treatment on corrosion properties.

RESULTS AND DISCUSSION

Microstructure Characterization

The XRD spectra of the as-printed DMLS-AlSi10Mg_200C sample and the heat-treated ones are presented in Figure 1, revealing strong texture in the (200) plane of the α -Al matrix. Peaks of Mg₂Si and Si were also identified. Based on Vegard's law, increasing the annealing temperature reduces Si solid solubility in Al matrix (Ma et al., 2014). Likewise, XRD patterns confirmed that increasing the heat-treatment temperature from 200 to 350°C expands the Si peaks' intensity, corresponding to the increased volume fraction of Si precipitate in the matrix. Moreover, Mg₂Si peak of the as-printed sample is lower than the heat-treated ones, which is associated with the reaction of the precipitated Si during heat-treatment with residual Mg available in the matrix and formation of Mg₂Si phase. As a result, Mg₂Si peak increases by raising the annealing temperature until there is no more Mg left in the matrix to precipitate in the form of Mg₂Si phase (Li et al., 2016).

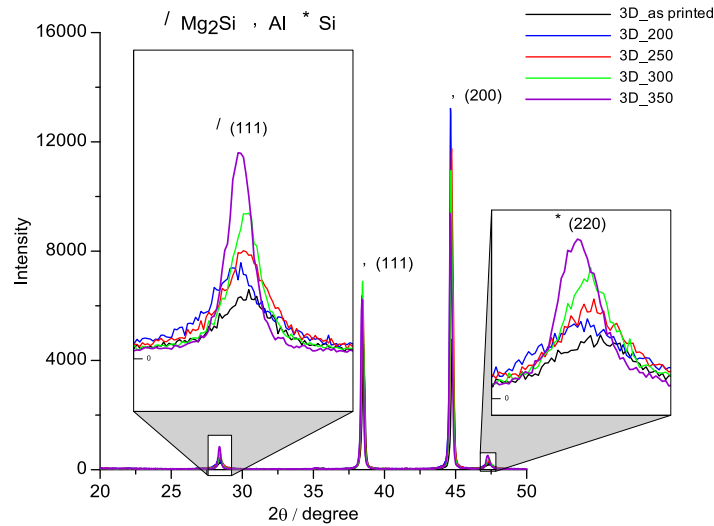


Figure 1. X-ray diffraction spectra of the DMLS-AISi10Mh_200C samples before and after annealing at different temperatures.

Figure 2 shows optical micrographs of the DMLS-AISi10Mg_200C sample in the as-printed condition a) parallel (side view) and b) perpendicular (top view) to the building direction, confirming a proper overlapping and densification between melt pools. Melt pools have a semi-circle shape, which their sizes depend on the laser beam parameters, *i.e.* the laser power and the scanning speed. Besides, Figure 2b shows irregular melt pools geometries and directions, which was attributed to 67° rotation of the laser scan between consecutive layers (Thijs, Kempen, Kruth, & Humbeeck, 2013). The optical microscopy investigation also confirmed that the performed low-temperature annealing in this study does not affect the overall macrostructure and morphology of the melt pools in the as-printed sample.

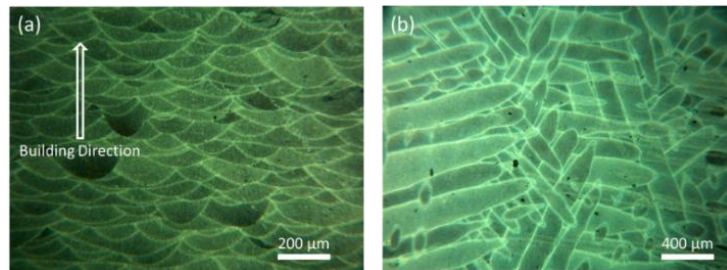


Figure 2. Optical micrographs of DMLS-AISi10Mg_200C sample, a) side view, along the building direction and b) top view, perpendicular to the building direction.

To further investigate the microstructure of the as-printed AISi10Mg_200C after low-temperature annealing, scanning electron microscopy analysis was employed. Figures 3 and 4 show the SEM images of the side and top views, respectively, of the DMLS-AISi10Mg_200C after annealing at various temperatures. Over the melt pool, in Figures 3a and 4a, there are three distinguishable regions with distinct microstructures formed by the moving heat source, *i.e.* fine cellular structure, coarse cellular structure, and transition heat affected zone (HAZ) structure that forms due to the overlapping scanning lines and layer-by-layer solidification of material (Li et al., 2015). It should be noted that critical solidification parameters, *i.e.* temperature gradient (G) and solidification rate (R), dictate the microstructure for a given composition (Kurz & Fisher, 1986). These values vary from the melt pool borders towards its center, resulting in a fine cellular-dendritic morphology in the melt pool center, where G is maximum and R is minimum during

solidification, and more elongated and coarser dendritic structure along the melt pool boundaries, where experience the lowest temperature gradient and the highest cooling rate.

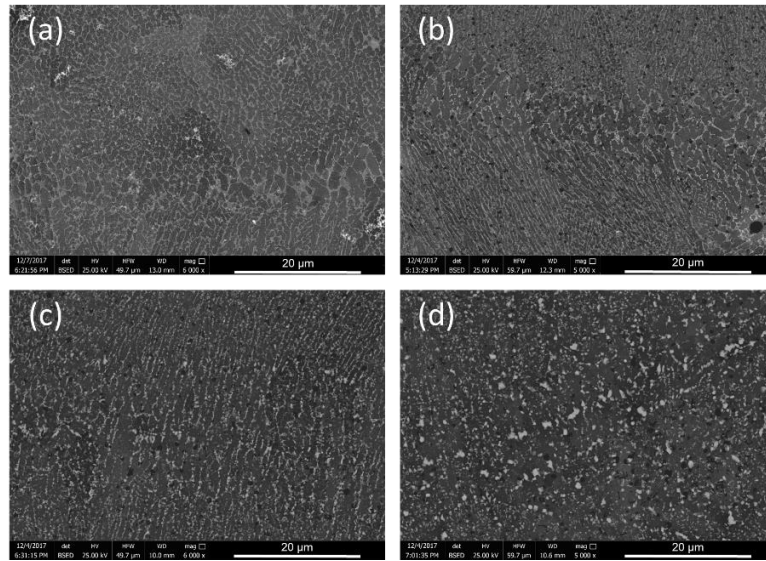


Figure 3. Side view SEM micrographs of the DMLS- $\text{AlSi10Mg}_{200\text{C}}$ heat-treated at a) 200°C, b) 250°C, c) 300°C, and d) 350°C.

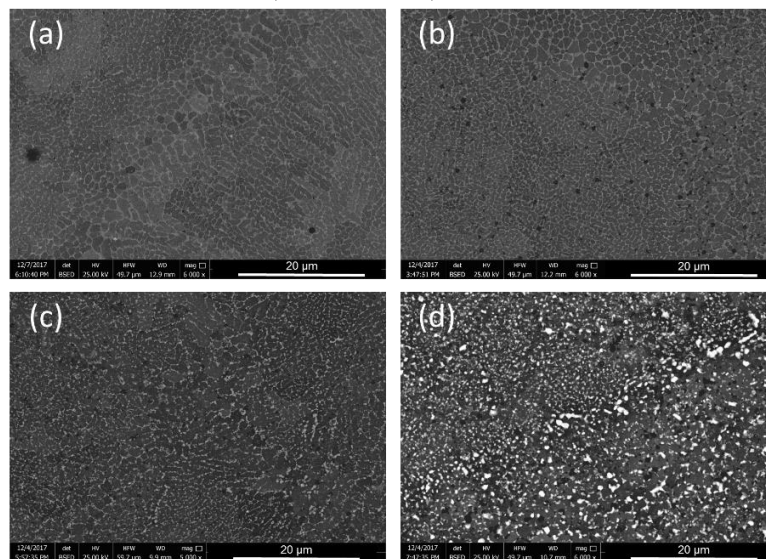


Figure 4. Top view SEM micrographs of the DMLS- $\text{AlSi10Mg}_{200\text{C}}$ heat-treated at a) 200°C, b) 250°C, c) 300°C, and d) 350°C.

Figures 3 and 4 also show evolving of the Si network morphology in the DMLS- $\text{AlSi10Mg}_{200\text{C}}$ structure after various low-temperature annealing treatments from the side and top views, respectively. The SEM micrographs revealed that by increasing the heat-treatment temperature from 200 to 350°C, the light grey intercellular Si network is broken by the growth of silicon phase into idiomorphic particles (see Figures 3d and 4d, resulting in an obscured Si network boundaries. Uniform precipitation of Si particles was also detected along the intercellular boundaries with the increase in the annealing temperature, which was found to be consistent with the results reported in a previous study (Li et al., 2016), giving rise to a more uniform microstructure than that of the as-printed $\text{AlSi10Mg}_{200\text{C}}$ sample (Cabrini et al., 2016). In

another study (Fiocchi, Tuissi, Bassani, & Biffi, 2017), two isothermal transformation temperatures were reported for the DMLS- AlSi10Mg alloy using differential scanning calorimetry, *i.e.* one at 263°C , corresponded to Si diffusion and Mg_2Si precipitation, and the other one around 294°C , related to the rupture and interruption of the Si network. Therefore, annealing at 250°C is almost the start of the Si diffusion and precipitation of Mg_2Si phase. By further increase in aging temperature, around 300°C , the continuous Si network starts to break. As evidenced by the XRD results shown in Figure 1, the rejected Si reacts with residual Mg in the matrix and precipitates in the form of Mg_2Si . Consequently, Mg_2Si peak intensity rises by increasing the heat-treatment temperature. Therefore, low-temperature heat-treatment around 300°C is the starting point for Si network breakage, resulting in a uniform dispersion of Si over the $\alpha\text{-Al}$ matrix.

Potentiodynamic Polarization Results

Figure 5 shows potentiodynamic polarization curves of the low-temperature heat-treated samples in fully polished condition. Previous studies have shown a lower corrosion resistivity on the side view (parallel to the building direction) of the DMLS- AlSi10Mg than that of the top view, which was reported to be associated with the higher density of the melt pools boundaries containing an increased content of Si and breakage of the Si network along the heat affected zone (Cabrini et al., 2016). For this reason, in this study, electrochemical properties of the samples were only measured from the side views.

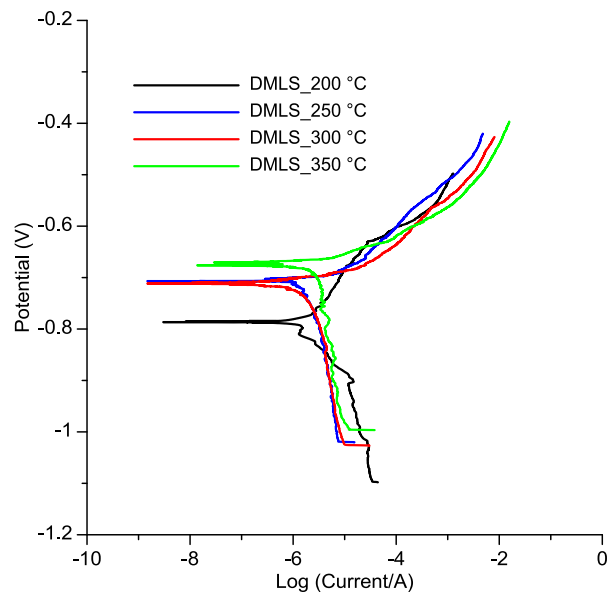


Figure 5. Tafel plot comparing the corrosion behavior of DMLS samples at four different heat-treatment temperatures.

Table 2 also shows all the results extracted from the Tafel plots shown in Figure 5, including the corrosion potential (E), corrosion current density (I), and corrosion rate of each of the heat-treated DMLS samples. Potentiodynamic polarization data demonstrate that increasing the heat-treatment temperature from 200 to 350°C decreases the corrosion rate of DMLS- $\text{AlSi10Mg}_{200\text{C}}$.

Table 2. Potentiodynamic polarization parameters of the heat-treated DMLS samples in 3.5 wt.% NaCl solution

	DMLS-200°C	DMLS-250°C	DMLS-300°C	DMLS-350°C
E. Corr. (V)	-0.7017	-0.7367	-0.7584	-0.6714
I Corr. (A/cm ²)	8.490 E-6	5.255 E-6	4.519 E-6	3.541 E-6
Corr. Rate (mm/y)	0.09768	0.06046	0.05199	0.04073

To investigate the severity and morphology of the corrosion attack, the surface of the samples were studied using SEM after corrosion products removal. Figure 6 shows the SEM images from the 200 and 350°C heat-treated DMLS-AISi10Mg_200C surface after the potentiodynamic polarization test. As shown in Figures 6a and 6b, a penetrating selective corrosion attack was detected for the 200°C heat-treated sample that preferentially expanded along the melt pools borders. On the other hand, the 350°C heat-treated sample, Figure 6c and 6d, behaved differently and showed a localized corrosion in the Al matrix around the periphery of the Si particles, but without a penetrating selective attack. This is ascribed to the uniform distribution of Si particles within the α -Al matrix in the 350°C heat-treated sample as opposed to the higher concentration of this phase precipitated along the melt pool boundaries of the 200°C heat-treated sample.

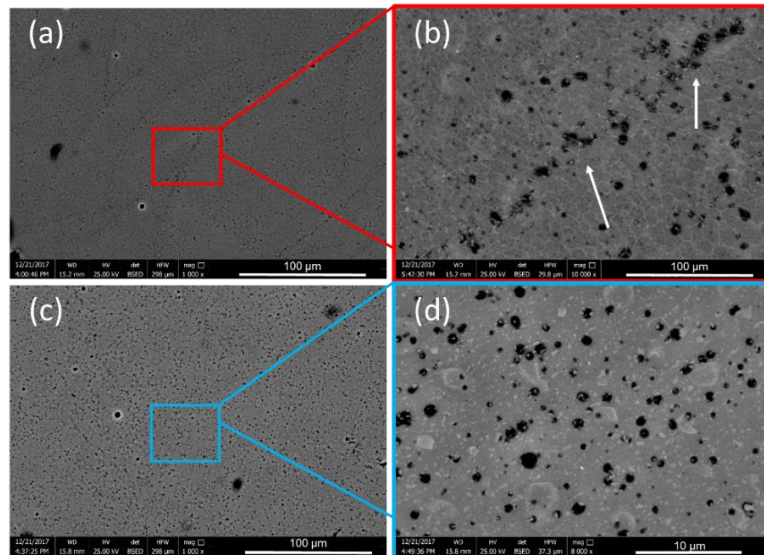


Figure 6. SEM images from the surface of the heat-treated DMLS-AISi10Mg_200C annealed at a) and b) 200°C, c) and d) 350°C, after the potentiodynamic polarization test and corrosion product removal.

Although the applied heat-treatment cycle resulted in the interruption of the Si network and boosted the precipitation of Si from supersaturated α -Al matrix, the improved uniformity of the microstructure avoided penetrating selective corrosion attacks and resulted in lowering the corrosion rate. Furthermore, heat-treatments can significantly modify the passive layer characteristics by increasing passive layer thickness as well as the oxide crystallinity (Cabrini et al., 2016). However, thermally formed passive layers might develop a micro-cracked structure containing porosities, resulting in a less protective behavior compare to naturally formed amorphous passive films (Vargel, 2004). To further investigate the protectiveness of the formed passive layer after the low temperature annealing treatments in this study, the EIS tests were conducted.

Electrochemical Impedance Spectroscopy (EIS) Results

Figure 7 shows the modification of the EIS spectra over time within five consecutive days. The constant high-frequency impedance values in the Bode plots are following the ohmic drop in the electrolyte. However, impedance differences in middle-low frequency ranges are more evident for different heat-treatment temperatures. At low frequencies, as a general trend, the modulus of impedance decreases by longer immersion time. On the contrary, modulus of impedance by increasing annealing temperature was found to be increased, confirming a slower kinetic for corrosion reactions. This is in agreement with the obtained potentiodynamic polarization results, confirming the lowest corrosion rate for the DMLS-AISi10Mg_200C sample aged at 350°C. This indicates an improvement in the protective nature of the passive layer formed during low-temperature annealing.

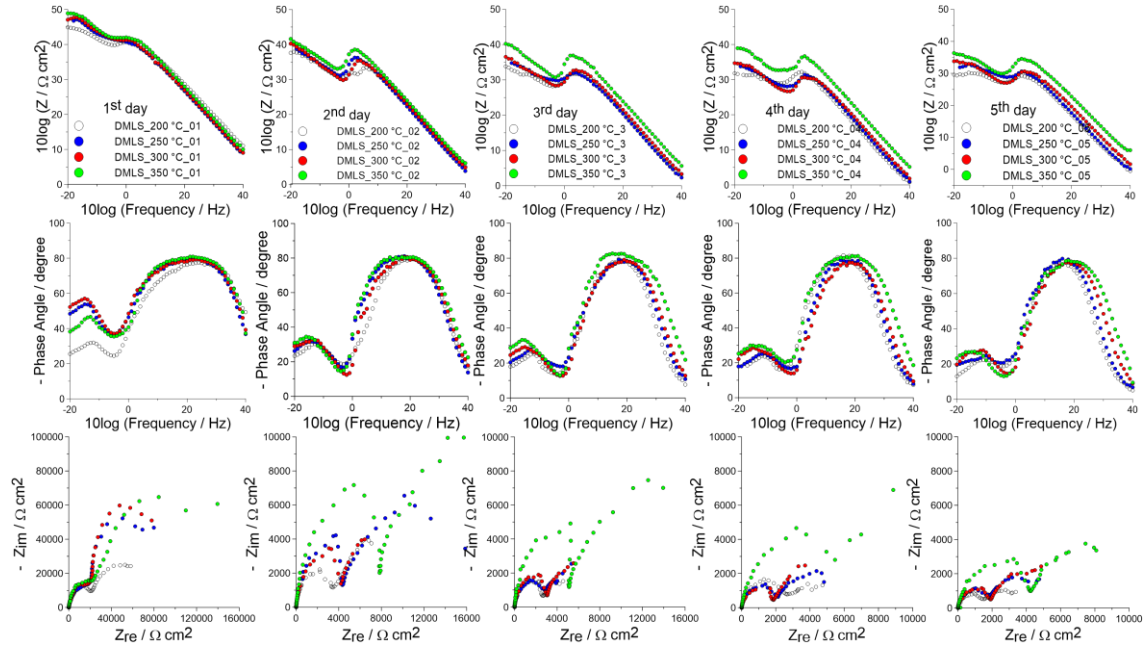


Figure 7. EIS spectra of DMLS-AlSi10Mg_200C after annealing heat-treatment at various temperatures in 3.5 wt.% NaCl solution.

It was reported that untreated DMLS-AlSi10Mg sample show one broad peak in the phase angle vs. frequency diagram in early immersion, composed of two different peaks with a non-evident time constant (Cabrini et al., 2016), typical of passive aluminum. However, after the heat-treatment, the phase angle vs. frequency diagrams were characterized by two different capacitive peaks with well-defined time constants in intermediate frequency range since early immersion. The low-frequency peak describes diffusion within corrosion products and within localized and selective attack zones, while the high-frequency peak displays sealing of the corrosion products inside porosity (Cabrini et al., 2016). It is also worth mentioning that the frequencies of the distinct peaks were constant, independent from the heat-treatment temperatures or the exposure time.

By increasing annealing temperature from 200 to 350°C, DMLS-AlSi10Mg_200C samples showed an improved passive behavior, as evidenced by the increased absolute value of impedance at low frequencies. Therefore, increasing annealing temperature from 200 to 350°C promotes uniformity of the microstructure by interrupting the Si network formed during the fabrication process of the DMLS-AlSi10Mg_200C and eliminates the silicon rich bands from the melt pool boundaries, which was found to be prone to the penetrating selective attack. Accordingly, the low-temperature annealing at 250 and 300°C showed an intermediate behavior, having a higher absolute value of impedance than that of the 200°C and lower than that of the 350°C heat-treated sample, which was again in agreement with the corrosion rate data. Consequently, the impedance response was improved, indicating an enhanced corrosion resistance. These findings are not consistent with the results reported in a previous study (Cabrini et al., 2016), where the authors reported a slight decrease of the corrosion potential of the DMLS-AlSi10Mg samples after annealing for four hours at 550°C. This high-temperature heat-treatment resulted in a significant coarsening of the Si particles, which was reported to cause a severe localized corrosion attack in the Al matrix at the periphery of the coarse Si particles. Although the applied heat-treatment in this study promoted Si precipitation and its network breakage, their size remains much smaller than the coarse Si particles that was formed by high-temperature heat-treatment process in the previous study (Cabrini et al., 2016). Hence, the improved corrosion performance in this study by low-temperature annealing treatment was contributed to the uniformity in distribution of the fine Si particles, which inhibited penetrating selective attack along the melt pool boundaries, despite localized corrosion evolved.

CONCLUSIONS

In this study, the effects of low temperature heat-treatment cycles on microstructure and electrochemical behavior of the DMLS-produced AlSi10Mg_200C in a 3.5 wt.% NaCl electrolyte were investigated. The as-printed samples were annealed at various temperatures. Microstructural analysis results confirmed that increasing annealing temperature from 200°C to 350°C resulted in an increased content of Si and interruption of the intercellular Si network in the structure, accompanied by an increased volume fraction of precipitated Mg₂Si phase in the structure. Therefore, uniformity of the microstructure, including size and distribution of Si particle in aluminum matrix was promoted by the increase in the annealing temperature. This microstructural modification was found to directly impact the corrosion performance of the alloy. The electrochemical measurements, *i.e.* Potentiodynamic polarization and EIS tests, confirmed improvement of the alloy's corrosion resistivity with a reduced susceptibility to penetrating selective attack as evidenced by the reduced corrosion rate and formation of a more protective passive film on the alloy with a higher value of impedance, by increasing annealing temperature from 200 to 350°C. Corrosion morphology was found to change from a penetrating selective attack along the melt pool boundaries for the DMLS-AlSi10Mg_200C sample annealed at 200°C to a more localized corrosion in the α -Al matrix surrounding the uniformly distributed Si particles when annealed at 350°C. Therefore, the uniformity of the microstructure of the DMLS-AlSi10Mg_200C resulted from a low temperature annealing heat-treatment was found to play a key role in dictating the material's corrosion behavior rather than the size of the Si particles.

ACKNOWLEDGMENTS

The authors wish to acknowledge the support of Natural Sciences and Engineering Research Council of Canada (NSERC) [grant number RGPIN-2017-04368], for sponsoring this work. M.M. would like to specially thank New Brunswick Innovation Foundation (NBIF) [grant number RIF2017-071] for providing funding to conduct this research.

REFERENCES

- Aboulkhair, N. T., Tuck, C., Ashcroft, I., Maskery, I., & Everitt, N. (2015). On the Precipitation Hardening of Selective Laser Melted AlSi10Mg. *Metallurgical and Materials Transactions A*, 46(8), 3337–3341. <https://doi.org/10.1007/s11661-015-2980-7>
- Asgari, H., Baxter, C., Hosseinkhani, K., & Mohammadi, M. (2017). On microstructure and mechanical properties of additively manufactured AlSi10Mg_200C using recycled powder. *Materials Science and Engineering: A*, 707(Supplement C), 148–158. <https://doi.org/https://doi.org/10.1016/j.msea.2017.09.041>
- Cabrini, M., Lorenzi, S., Pastore, T., Pellegrini, S., Ambrosio, E. P., Calignano, F., ... Fino, P. (2016). Effect of heat treatment on corrosion resistance of DMLS AlSi10Mg alloy. *Electrochimica Acta*, 206(Supplement C), 346–355. <https://doi.org/https://doi.org/10.1016/j.electacta.2016.04.157>
- Cabrini, M., Lorenzi, S., Pastore, T., Pellegrini, S., Manfredi, D., Fino, P., ... Badini, C. (2016). Evaluation of corrosion resistance of Al–10Si–Mg alloy obtained by means of Direct Metal Laser Sintering. *Journal of Materials Processing Technology*, 231(Supplement C), 326–335. <https://doi.org/https://doi.org/10.1016/j.jmatprotec.2015.12.033>
- Fiocchi, J., Tuissi, A., Bassani, P., & Biffi, C. A. (2017). Low temperature annealing dedicated to AlSi10Mg selective laser melting products. *Journal of Alloys and Compounds*, 695(Supplement C), 3402–3409. <https://doi.org/https://doi.org/10.1016/j.jallcom.2016.12.019>
- Fulcher, B. A., Leigh, D. K., & Watt, T. J. (2014). Comparison of AlSi10Mg and Al 6061 processed through DMLS. In *Proceedings of the Solid Freeform Fabrication (SFF) Symposium, Austin, TX, USA* (Vol. 46).

- Kurz, W., & Fisher, D. J. (1986). *Fundamentals of solidification* (Vol. 1). trans tech publications Aedermannsdorf, Switzerland.
- Li, B., Wang, H., Jie, J., & Wei, Z. (2011). Effects of yttrium and heat treatment on the microstructure and tensile properties of Al-7.5Si-0.5Mg alloy. *Materials & Design*, 32(3), 1617–1622. <https://doi.org/https://doi.org/10.1016/j.matdes.2010.08.040>
- Li, W., Li, S., Liu, J., Zhang, A., Zhou, Y., Wei, Q., ... Shi, Y. (2016). Effect of heat treatment on AlSi10Mg alloy fabricated by selective laser melting: Microstructure evolution, mechanical properties and fracture mechanism. *Materials Science and Engineering: A*, 663(Supplement C), 116–125. <https://doi.org/https://doi.org/10.1016/j.msea.2016.03.088>
- Li, X. P., Wang, X. J., Saunders, M., Suvorova, A., Zhang, L. C., Liu, Y. J., ... Sercombe, T. B. (2015). A selective laser melting and solution heat treatment refined Al-12Si alloy with a controllable ultrafine eutectic microstructure and 25% tensile ductility. *Acta Materialia*, 95(Supplement C), 74–82. <https://doi.org/https://doi.org/10.1016/j.actamat.2015.05.017>
- Ma, P., Prashanth, K. G., Scudino, S., Jia, Y., Wang, H., Zou, C., ... Eckert, J. (2014). Influence of Annealing on Mechanical Properties of Al-20Si Processed by Selective Laser Melting. *Metals*, 4(1), 28–36. <https://doi.org/10.3390/met4010028>
- Manfredi, D., Ambrosio, E. P., Calignano, F., Krishnan, M., Canali, R., Biamino, S., ... Badini, C. (2013). Direct Metal Laser Sintering: an additive manufacturing technology ready to produce lightweight structural parts for robotic applications. *La Metallurgia Italiana*, 10.
- Mertens, A., Dedry, O., Reuter, D., Rigo, O., & Lecomte-Beckers, J. (2015). Thermal treatments of AlSi10Mg processed by laser beam melting. In *Proceedings of the 26th International Solid Freeform Fabrication Symposium* (pp. 1007–1016).
- Thijs, L., Kempen, K., Kruth, J., & Humbeeck, J. V. (2013). Fine-structured aluminium products with controllable texture by selective laser melting of pre-alloyed AlSi10Mg powder. *Acta Materialia*, 61(5), 1809–1819. <https://doi.org/https://doi.org/10.1016/j.actamat.2012.11.052>
- Vargel, C. (2004). *Corrosion of Aluminium*. Oxford, UNKNOWN: Elsevier Science. Retrieved from <http://ebookcentral.proquest.com/lib/mun/detail.action?docID=288714>